The Mechanism of Charge-transfer Nitration of Naphthalene

Eun K. Kim, T. Michael Bockman and Jay K. Kochi
Chemistry Department, University of Houston, Houston, TX 77204-5641, USA

Electrophilic (thermal) and charge-transfer (photochemical) nitration of naphthalene are effectively carried out in acetonitrile with various X-substituted *N*-nitropyridinium salts with X = 4-MeO, H, 4-MeO_2C and 2,6-Me_2. Quantitative analyses indicate that both processes effect nuclear nitration to afford the same distribution of isomeric α- and β-nitronaphthalenes, together with the production of various amounts of (nitro-pyridine) adducts to naphthalene. Time-resolved (picosecond) spectroscopy identifies the naphthalene cation radical ($NAPH^{\bullet+}$) as the critical reactive intermediate in charge-transfer nitration. The subsequent disappearance of $NAPH^{\bullet+}$ occurs by its combination with NO_2 to form the isomeric (α/β) Wheland intermediates, which suffer competitive deprotonation (to yield the nitronaphthalenes) and nucleophilic addition (to produce the adducts). The relevance of such a charge-transfer mechanism to naphthalene nitration *via* the electrophilic (thermal) process is discussed.

N-Nitropyridinium salts are versatile reagents for the *electrophilic* (thermal) nitration of different types of aromatic donor (ArH), particularly in neutral (aprotic) solvents such as acetonitrile.[1] For mechanistic studies of aromatic nitration, it is singularly important that the electronic and steric properties of the active electrophile ($X\text{-}PyNO_2^+$) are strongly modulated by a substituent (X) on the *para* and *ortho* positions, respectively, of the heteroaromatic ring.[2] *N*-Nitropyridinium cations are also effective in the alternative *charge-transfer* (actinic) nitration of the same aromatic donors by the deliberate photo-excitation ($h\nu_{CT}$) of the pre-equilibrium (EDA) complex,[3] eqns. (1) and (2).

$$ArH + X\text{-}PyNO_2^+ \overset{K_{EDA}}{\rightleftharpoons} [ArH, X\text{-}PyNO_2^+] \quad (1)$$

$$[ArH, X\text{-}PyNO_2^+] \xrightarrow{h\nu_{CT}} ArNO_2 + X\text{-}PyH^+ \quad (2)$$

Both processes are carried out under essentially the same experimental conditions—the photochemical (charge-transfer) nitration being merely effected at lower temperatures where competition from electrophilic nitration is unimportant. Consequently, any mechanistic insight obtained about charge-transfer nitration will bear directly on the mechanism of electrophilic aromatic nitration.[4,5]

Various naphthalene donors have been the subject of numerous mechanistic studies[4,5] which have focused on the isomeric (α/β) nitronaphthalenes, sidechain substitutions and the *ipso* adducts—especially as they relate to the possible role of cation radicals[6] in electrophilic aromatic nitration.[7–10] Although the study of such reactive intermediates as aromatic cation radicals has heretofore been based largely on indirect experimental methods, it is now possible to examine them by direct spectroscopic methods.[11,12] Indeed we employed time-resolved spectroscopy in the foregoing study[13] to show that the aromatic cation radical $DMN^{\bullet+}$ is the reactive intermediate in the charge-transfer (CT) activation of the EDA complex *via* the triad in eqn. (3) as it is evolved into the *ipso* adduct in 1,4-

$$[DMN, PyNO_2^+] \xrightarrow[CH_3CN]{h\nu_{CT}} [DMN^{\bullet+}, NO_2, Py] \; etc. \quad (3)$$

dimethylnaphthalene (DMN) nitration and sidechain substitution. Accordingly, we now focus on the mechanism of the charge-transfer nitration of naphthalene itself with three principle objectives in mind: (*a*) to compare quantitatively the isomeric (α/β) nitronaphthalenes with those produced under comparable conditions *via* electrophilic nitration with $X\text{-}PyNO_2^+$, in which the pyridine moiety is either a relatively strong base (X = 4-methoxy), a weak base (X = 4-methoxycarbonyl), or a hindered base (X = 2,6-dimethyl); (*b*) to observe the naphthalene cation radical as the critical intermediate by time-resolved spectroscopy on both the picosecond and nano-/micro-second timescales, and to follow its decay kinetics in the formation of the isomeric (α/β) nitronaphthalenes as they are affected by the structure and concentration of the pyridine base; and (*c*) to establish the mechanism of charge-transfer nitration of naphthalene (with due cognizance of the *ipso* and related adducts)[3,14] and to relate these mechanistic conclusions to the electrophilic nitration of naphthalene.

In order to provide perspective to the charge-transfer study of naphthalene with *N*-nitropyridinium, parallel experiments were also carried out with the tetranitromethane (TNM) acceptor for which the charge-transfer nitration of related aromatic donors has been previously delineated.[15]

Results

Pure nitronium tetrafluoroborate, free of any nitrosonium adulterant, was converted into the crystalline *N*-nitropyridinium salt at −20 °C as described by Olah and coworkers.[1] Essentially the same procedure was also used to prepare the various analogues[2] (Scheme 1) where X = 4-methoxy, hydrogen, 4-methoxy-

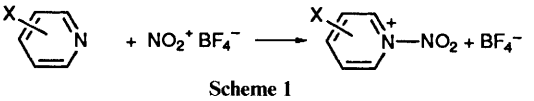

Scheme 1

carbonyl and 2,6-dimethyl substituents as colourless, hygroscopic crystals that were always manipulated in a moisture-free glovebox (see the Experimental section).

Electrophilic Nitration of Naphthalene with N-*Nitropyridinium Salts.*—When naphthalene was added to *N*-nitro-2,6-lutidinium tetrafluoroborate in the dark at −20 °C, the colourless solution immediately turned bright yellow. The colour gradually faded over the course of half an hour as the acetonitrile solution was allowed to warm to *ca.* 0 °C. The subsequent spectral (^1H NMR) analysis of the clear pale solution indicated the presence of hydrolutidinium, and a

Table 1 Electrophilic nitration of naphthalene with *N*-nitropyridinium salts[a]

X-PyNO$_2$$^+$[b]			Nitronaph. (μmol)					
X	μmol	Naph. (μmol)	α	β	α/β[c]	Conv. (%)[d]	*T*/°C	*t*/h
2,6-Me$_2$	99	60	43	6.6	87/13	83[e]	−20 ~ 0	0.5
4-MeO$_2$C	94	50	38	3.0	93/7	86[f]	23	0.03
H	25	45	11	1.4	89/11	60[g]	23	21
H[h]	300	150	133	13.5	91/9	98	25	—
HNO$_3$[h]	2500	2000	1880	120	94/6	94	0	0.2

[a] In acetonitrile solutions in the dark, unless indicated otherwise. [b] As tetrafluoroborate salt, unless indicated otherwise. [c] Molar ratio. [d] Based on naphthalene consumed. [e] Recovered naphthalene was <0.1. [f] 7.2. [g] 30 μmol. [h] Nitric acid, from ref. 3.

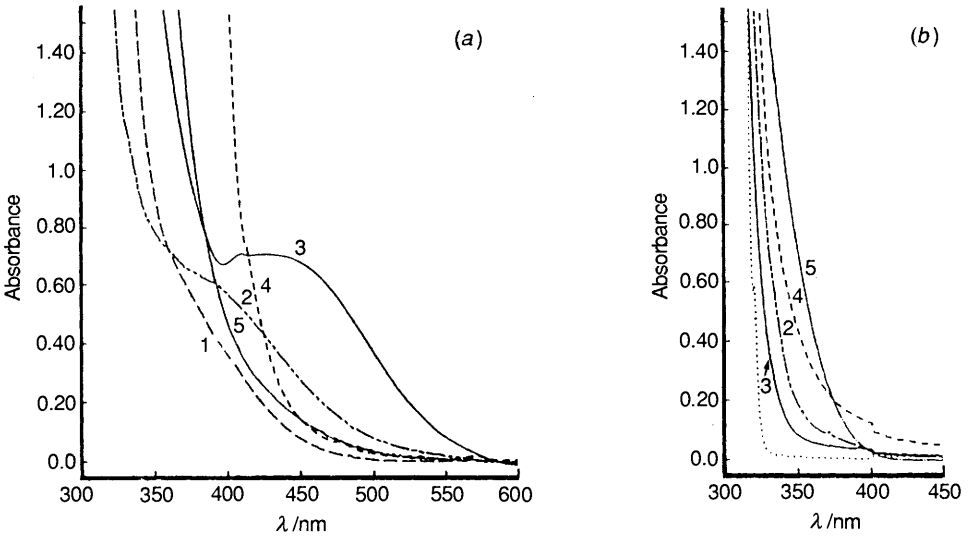

Fig. 1 (*a*) Charge-transfer spectra of the naphthalene complex with either X-PyNO$_2$$^+$ for X = 4-methoxy (1), hydrogen (2), 4-methoxycarbonyl (3), and 2,6-dimethyl (4) or tetranitromethane (5) in acetonitrile. (*b*) Absorption spectra of the nitrating agents alone (as indicated) and naphthalene alone (· · · · · · ·) in acetonitrile.

mixture of α- and β-nitronaphthalenes according to the metathetical reaction in eqn. (4) (see the Experimental section

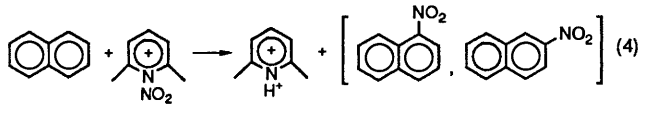

(4)

for details). Upon the addition of ether, the lutidinium salts separated from solution, and the resulting mother liquor consisting of a mixture of nitronaphthalenes was quantitatively analysed (Table 1) by both high pressure liquid chromatography (HPLC) and gas chromatography–mass spectroscopy (GC–MS) using the internal standard method.

In order to examine the temperature effect, naphthalene was treated with the reactive *N*-nitro-4-methoxycarbonylpyridinium salt[2] at 23 and −15 °C, and the same high yields of α-nitronaphthalene (90 ± 3%) and β-nitronaphthalene (10 ± 3%) were consistently obtained over a *ca.* 40 °C temperature range. The nitration of naphthalene with the highly electrophilic *N*-nitro-4-methoxycarbonylpyridinium salt (entry 2) thus parallels that of the parent *N*-nitropyridinium salt (entry 3) and nitric acid/acetic anhydride (entry 5) from the previous studies.[2,3] When these nitrating agents were replaced by tetranitromethane, no thermal reaction was apparent (in the dark for days), and the charge-transfer absorption spectrum of the yellow solution was undiminished.

Charge-transfer Nitration of Naphthalene by Irradiation of the EDA Complexes.—The bright yellow solution of naphthalene and nitro-2,6-lutidinium salt (described in the foregoing section) persisted unchanged for prolonged periods if the temperature was maintained below −40 °C. Accordingly, the yellow solution was deliberately irradiated at this temperature with the focused output of a 500-W mercury–xenon lamp equipped with a sharp (Pyrex) cut-off filter (Corning CS series) to remove all extraneous light with $\lambda < 410$ nm. Inspection of the absorption spectrum in Fig. 1 ensured that such filtered light could selectively excite only the charge-transfer absorption band of the naphthalene EDA complex with *N*-nitrolutidinium; and the possibility of the adventitious excitation of either the uncomplexed naphthalene or *N*-nitrolutidinium cation was thus precluded. The ^{1}H NMR spectrum of the photolysate was monitored periodically, and after high photochemical conversion had been achieved (Table 2), it was found to be virtually identical with that of the reaction mixture obtained by electrophilic nitration of naphthalene in eqn. (4). Indeed, the standard work-up of the photolysate by ether addition led to the separation of the lutidinium salts from the nitronaphthalene mixture, which upon quantitative HPLC analysis revealed excellent yields of α and β isomers according to the stoichiometry in eqn. (5). The control experiment carried out

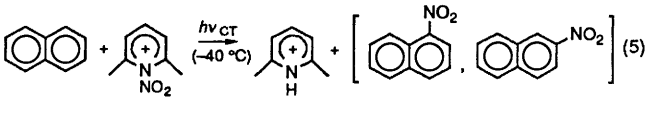

(5)

simultaneously in the dark established the absence of any electrophilic (thermal) component to naphthalene nitration under the charge-transfer conditions described in eqn. (5). Essentially the same results were obtained in the charge-transfer

Table 2 Charge-transfer nitration of naphthalene by irradiation of the X-$PyNO_2^+$ and TNM complexes[a]

X-$PyNO_2^+$			Naph.	λ_{exc}[b]	Nitronaph. (μmol)			Rec.[c]	Conv.[d]		
No.	X	μmol	(μmol)	nm	α	β	α/β	(μmol)	(%)	T/°C	t/h
1	2,6-Me_2	43	90	410	19.7	1.1	95/5	63	93	−40	16
2	4-MeO_2C	92	100	500	42	4.3	91/9	53	51	−40	12
3	4-MeO	82	85	425	23	1.7	93/7	47	46	23	7
4	4-MeO	100	50	380	33	1.3	96/4	5	90[g]	−40	4
5	4-MeO[e]	100	100	425	62	4.7	93/7	17	83	23	11
6	4-MeO	100	85	425[f]	25	1.4	95/5	53	38	23	15
7	H	30	70	425	11	1.9	86/14	42	93	−40	10
Tetranitromethane											
8	TNM	217	91	480	10.7	0.5	95/5	27	70	23	4
9	TNM[h]	217	109	480	4.7	0.6	89/11	<0.2	99	23	16
10	TNM[e]	217	100	425	49	2.4	95/5	2	98	23	15

[a] In acetonitrile solution by CT excitation with λ_{exc}, unless indicated otherwise. [b] High-energy cut-off. [c] Recovered naphthalene. [d] Conversion based on naphthalene consumed. Includes adducts, see Table 3. [e] With 5 vol.% trifluoroacetic acid added. [f] Diffuse light (see the text). [g] Adducts not included (undetermined). [h] In chloroform.

Table 3 Formation of naphthalene adducts and their hydrolytic elimination[a]

	Nitrating		Naph.	λ_{exc}	Adducts[c]	Nitronaphthalenes[d]		
No.[b]	agent	μmol	(μmol)	nm	(μmol)	α	β	α/β
3	$MeOPyNO_2^+$	82	85	425	10	5	0.8	86/14
7	$PyNO_2^+$	30	70	425	10	6.4	0.7	90/10
2	$MeO_2CPyNO_2^+$	92	100	500	<0.4	*e*	*e*	*e*
1	$LutNO_2^+$	43	90	410	<0.1	*e*	*e*	*e*
8	TNM	217	91	480	50	26	15	64/36
9	TNM[f]	217	109	480	98	42	15	74/26
5	$MeOPyNO_2^+$[g]	100	100	425	<0.4	*e*	*e*	*e*
6	$MeOPyNO_2^+$	100	85	425[h]	3	3	0.3	90/10
	TNM	2500	150	425	130	78	36	68/32
10	TNM[g]	217	100	425	14	*e*	*e*	*e*

[a] In acetonitrile solution unless indicated otherwise. [b] Entry No. in Table 2. [c] As isomeric mixture. [d] Formed upon hydrolytic elimination of adduct mixture. [e] Not determined. [f] In chloroform. [g] In the presence of 5 vol% added trifluoroacetic acid. [h] Diffuse light (see the text).

nitration of naphthalene with the reactive 4-methoxycarbonyl analogue $MeO_2CPyNO_2^+$ (entry 2, Table 2).

The effect of temperature variation on charge-transfer nitration was examined with *N*-nitro-4-methoxypyridinium owing to its significantly lower electrophilic reactivity.[2] With this reagent, the charge-transfer nitration of naphthalene could be carried out at room temperature without competition from the electrophilic (thermal) process. As such, the results in Table 2 (entries 3 and 4) are noteworthy in that the same isomeric mixtures of α-nitronaphthalene (94 ± 2%) and β-nitronaphthalene (5 ± 2%) were obtained in charge-transfer nitration over a 60 °C range in temperature.

Formation of Naphthalene Adducts as By-products.—When the photolysate obtained from the charge-transfer nitration of naphthalene with *N*-nitro-4-methoxypyridinium (see Table 2, entry 3) was immediately subjected to direct ^1H NMR analysis, the nitronaphthalene mixture indicated the presence of an additional (minor) component. Since the diagnostic pair of resonances centred at δ 6.38 and 6.61 was characteristic of the vinylic proton signals at δ 6.42 and 6.45 previously observed for the *ipso* adduct **A** to 1,4-dimethylnaphthalene,[13] they were assigned to the corresponding naphthalene adduct **B**. Although

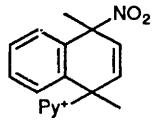

A

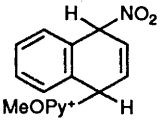

B

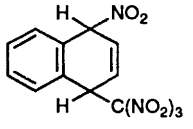

C

the cationic adduct **B** (and its isomers) were readily precipitated from solution upon the addition of ether, the small amounts obtained did not allow quantitative separation away from the other methoxypyridinium salts for separate analysis. Thus for the structural characterizations, we turned to the charge-transfer nitration of naphthalene with tetranitromethane, in which the structure of the analogous adduct **C** has been established by X-ray crystallography.[14] Indeed, the results in Table 3 (entry No. 8) show the simultaneous formation of the α/β-nitronaphthalenes and the adduct **C** (with vinyl protons in the ^1H NMR spectrum at δ 6.74 and 6.78) together with its isomers, eqn. (6). (Note for comparison, the vinylic proton

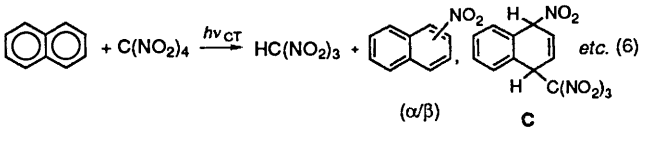

resonances in the *ipso* adduct of tetranitromethane to 1,4-dimethylnaphthalene are δ 6.41 and 6.62.)[3] The nitronaphthalene yields were significantly enhanced (at the expense of the adduct), when the charge-transfer nitration of naphthalene with tetranitromethane was carried out in acetonitrile solutions containing 5 vol% trifluoroacetic acid (see the last entry in Table 3). Under all circumstances, the isomeric composition of the α- and β-nitronaphthalenes remained remarkably invariant at 92 ± 3% and 8 ± 3%, respectively. Careful control experiments established that adduct **C** in eqn. (6) was stable under the

reaction conditions extant in charge-transfer nitration. It follows, therefore, that the yields of α- and β-nitronaphthalene in Table 2, however limited, always represented the isomeric composition resulting from the charge-transfer nitration of naphthalene with tetranitromethane.

When the adduct **C** (together with its isomers) was subsequently subjected to the hydrolytic elimination of nitroform (see the Experimental section), it afforded a mixture of α- and β-nitronaphthalenes with roughly the same isomeric composition as those listed in Table 2. It is noteworthy that a solution of crystalline *syn* isomer[14] of the 1,4-adduct **C** in acetonitrile was slowly converted only into α-nitronaphthalene upon the addition of water, or more rapidly by aqueous hydrogencarbonate solution.

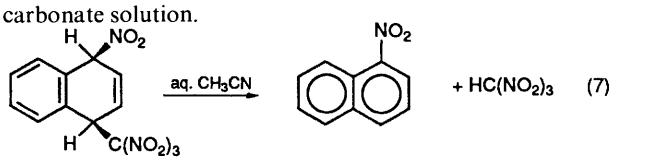

C

The spectral (^{1}H NMR) identification of the tetranitromethane adducts in eqn. (6) permitted a direct analysis of the analogous *N*-nitropyridinium adducts to naphthalene (see the Experimental section). Thus the more complete stoichiometry for the charge-transfer nitration of naphthalene with *N*-nitro-4-methoxypyridinium is that described in eqn. (8) and the

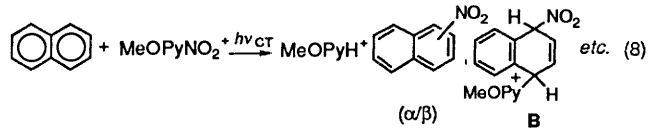

quantitative analysis is included in Tables 2 and 3 (see entry No. 3). Continued monitoring of the ^{1}H NMR spectrum of the reaction mixture indicated that the methoxypyridinium adducts in eqn. (8) were persistent under the conditions of the charge-transfer nitration described in Table 2. However, when allowed to stand for extended periods *in situ* (or more rapidly by the addition of aqueous hydrogencarbonate), the adduct mixture decomposed according to the stoichiometry given in eqn. (9) in

$$C_{10}H_8(NO_2)(MeOPy)^+ \longrightarrow \underset{\text{(B and isomers)}}{} \underset{(\alpha/\beta)}{C_{10}H_7NO_2} + MeOPyH^+ \quad (9)$$

which the isomeric (α/β) ratio of nitronaphthalenes was essentially that reported in Table 2 (entry 3). Interestingly, the amounts of adducts formed relative to the nitronaphthalenes in eqn. (8) could be deliberately altered in the following ways. First, adduct formation was completely suppressed when the charge-transfer nitration of naphthalene with $MeOPyNO_2^+$ was carried out in acetonitrile solutions containing 5 vol% trifluoroacetic acid, as presented in Table 3 (entry No. 5). (Control experiments established that the stability of the methoxypyridinium adducts was unaffected by trifluoroacetic acid under these conditions.) Second, the attenuation of the light flux across the face of the photochemical cell (by the simple removal of the focusing lens) also led to the reduction in adduct yield (entry No. 6). In both cases, the isomeric composition of the nitronaphthalene mixture was unaffected.

In order to establish the existence of analogous adducts with other nitropyridinium cations, the charge-transfer nitration of naphthalene with the parent *N*-nitropyridinium acceptor ($PyNO_2^+$) was repeated, and the photolysates spectrally examined at −40 °C. Indeed the presence of the diagnostic resonances of the vinylic protons (δ 6.41 and 6.58) indicated that adduct **B** (and isomers) were formed in *ca.* 20% yield. When the solution was warmed to room temperature, the ^{1}H NMR spectrum of the adduct was completely replaced by that of the isomeric (α/β) nitronaphthalenes [*cf.* eqn. (9)] over the course of *ca.* 12 h. Similarly, the charge-transfer nitration of naphthalene with *N*-nitro-4-methoxycarbonylpyridinium at −40 °C afforded only α- and β-nitronaphthalene, and no vinylic proton resonance at δ ~6.5 for the methoxycarbonylpyridine adduct (<5%) could be discerned. From such studies, we concluded that the series of X-substituted *N*-nitropyridinium acceptors afforded adducts with an increasing facility for hydrolytic elimination in the order: X = MeO < H < MeO_2C, according to the typical stoichiometry in eqn. (9). Furthermore, the weak nucleophile MeO_2CPy showed little propensity for adduct formation. Since the electrophilic reactivity of $X\text{-}PyNO_2^+$ followed the opposite trend,[2] with X = MeO being the least reactive, we were unable to establish any experimental conditions in which the electrophilic nitration could be carried out so that the (nitro-pyridine) adduct to the naphthalene could be simultaneously observed. Nonetheless, the partial results suggested that adduct formation was significantly less important in electrophilic nitration compared with charge-transfer nitration carried out under more or less comparable conditions.

Time-resolved (Picosecond) Spectroscopy of Naphthalene Cation Radicals as the Reactive Intermediates in Charge-transfer Nitration.—To identify the reactive intermediates responsible for charge-transfer nitration, we initially examined the time-resolved spectra of the transients following the application of a 30 ps (fwhm) laser pulse. The third harmonic at 355 nm of the mode-locked Nd^{3+}:YAG laser was used to excite the charge-transfer band. The absorption spectrum in Fig. 1 indicated that λ_{exc} = 355 nm would specifically excite only the naphthalene–EDA complex with nitropyridinium, and it could not lead to the local-band excitation of either the free (uncomplexed) aromatic donor or the cationic acceptor.

The 355 nm irradiation of the yellow solution of *N*-nitro-4-methoxypyridinium tetrafluoroborate and excess naphthalene in acetonitrile resulted immediately in an intense, broad absorption in the spectral region between 500 and 700 nm. At short times (50 ps) following the application of the laser pulse, the resolved spectrum in Fig. 2(*a*) consisted of the characteristic bands of the naphthalene cation radical ($NAPH^{\bullet+}$) with distinct maxima at λ_{max} 680, 660 and 625 nm.[16,17] Spectra acquired at the longer times of 200 and 400 ps showed the progressive diminution of the $NAPH^{\bullet+}$ absorption, and the concomitant growth of a broader (unresolved) band with λ_{max} = 575 nm. The latter was readily assigned to the dimer cation of naphthalene by its comparison with the authentic spectrum of $(NAPH)_2^{\bullet+}$ previously generated independently.[18,19] These spectral assignments were supported by parallel time-resolved studies carried out of the transients from the CT excitation of the naphthalene complex with tetranitromethane. Owing to the residual TNM absorbance at 355 nm (see Fig. 1), the second harmonic at 532 nm of the Nd^{3+}:YAG laser was used to excite the weak, low-energy tail. Notably, the series of transient spectra in Fig. 2(*b*) were the same as those obtained from the photo-excitation of the naphthalene EDA complex with the nitropyridinium acceptor in Fig. 2(*a*).

In the charge-transfer excitations of the naphthalene EDA complexes with nitropyridinium and tetranitromethane at λ_{exc} = 355 and 532 nm, respectively, only the dominant absorption band of the dimeric $(NAPH)_2^{\bullet+}$ was apparent after 5 ns—that of the monomeric $NAPH^{\bullet+}$ having decayed in this time interval to the spectral baseline. In both cases, the clean interconversion of naphthalene cation radicals according to

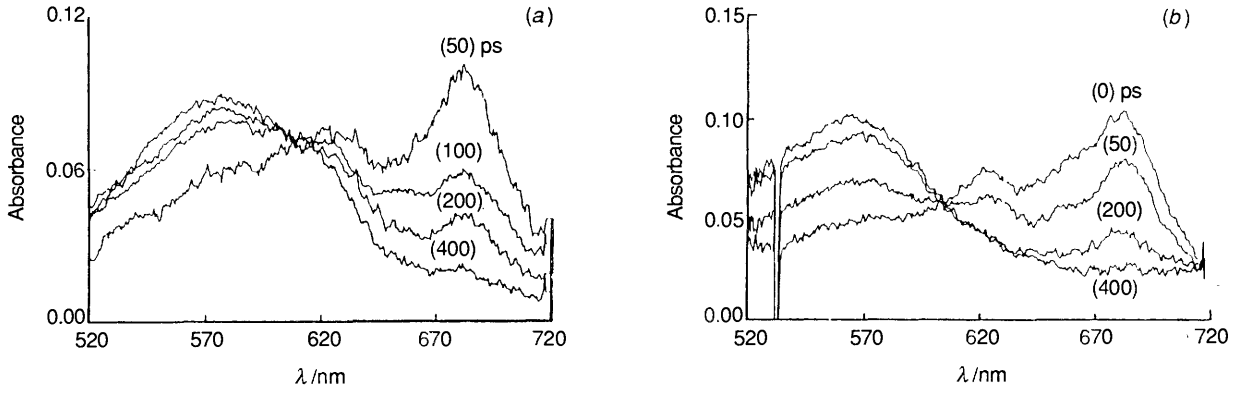

Fig. 2 Time-resolved picosecond absorption spectra of naphthalene cation radicals from the CT excitation of the naphthalene complex with (*a*) *N*-nitro-4-methoxy-pyridinium at 355 nm and (*b*) tetranitromethane at 532 nm. Temporal evolution of the transient spectra at intervals following the 30 ps laser pulse are indicated in parentheses.

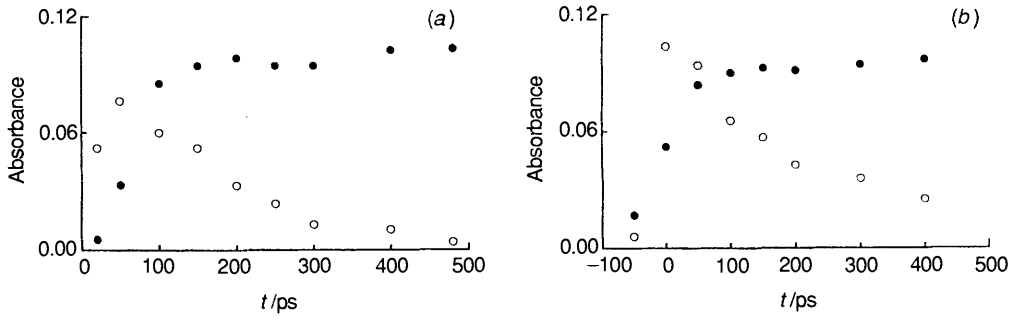

Fig. 3 Kinetics of the spectral decay of $NAPH^{\bullet+}$ (○) and the concomitant growth of $(NAPH)_2^{\bullet+}$ (●) at λ_{mon} = 678 and 580 nm, respectively, following the CT excitation of the naphthalene complex with (*a*) *N*-nitro-4-methoxypyridinium and (*b*) tetranitromethane in acetonitrile at 23 °C

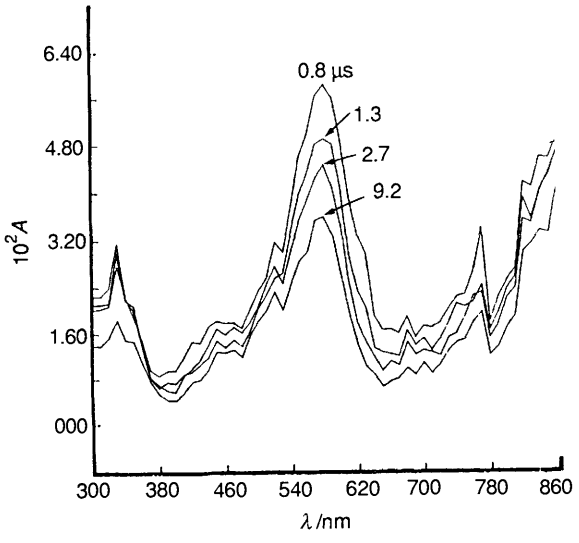

Fig. 4 Time-resolved nanosecond absorption spectra of $(NAPH)_2^{\bullet+}$ at the indicated times following the 355 nm excitation of 0.01 mol dm^{-3} $MeOPyNO_2^+$ and 0.2 mol dm^{-3} naphthalene in acetonitrile at 23 °C

eqn. (10) is shown in Fig. 2 by the presence of the single isosbestic point at λ = 605 nm.

$$NAPH^{\bullet+} + NAPH \overset{K}{\rightleftharpoons} (NAPH)_2^{\bullet+} \qquad (10)$$

The rate of the interconversion of naphthalene cation radicals was followed by monitoring the absorbance changes at λ_{max} = 678 and 581 nm of the monomeric and dimeric species, respectively. The pseudo-first-order decays of $NAPH^{\bullet+}$ shown in Fig. 3 corresponded to a second-order rate constant of k_a = $3 \pm 2 \times 10^{10}$ dm^3 mol^{-1} s^{-1}, as evaluated from the EDA complexes of both nitropyridinium and tetranitromethane with naphthalene in the concentration range 0.1–0.4 mol dm^{-3}. The calculated degree of dimer dissociation in eqn. (10) of $\alpha \approx 3\%$ for $(NAPH)_2^{\bullet+}$ (*vide infra*) is consistent with the decay of the 680 nm band of $NAPH^{\bullet+}$ to the baseline in Fig. 3.

Quantum Efficiency for the CT Generation of Naphthalene Cation Radicals from the EDA Complex.—In order to quantify the production of the naphthalene cation radicals (at the temporal plateau shown in Fig. 3), the charge-transfer excitations were carried out with a second spectrometric unit that consisted of a Q-switched Nd^{3+}:YAG laser with 10 ns (fwhm) resolution for spectral observations extending down into the microsecond region. The significantly wider spectral window allowed in the ns/μs measurements (see the Experimental section) also enabled the absorption spectra of the charge-transfer transients to be examined between 300 < λ < 900 nm. Thus the transient (ns) spectra in Fig. 4 show the principal absorption band of $(NAPH)_2^{\bullet+}$ with λ_{max} = 580 nm corresponding to that in the ps spectra in Fig. 2. In addition, the spectral features of $(NAPH)_2^{\bullet+}$ included the tail of the near-IR band (λ_{max} 1030 nm) and the weak visible (λ_{max} 530 nm) and UV (λ_{max} 320 nm) bands reported earlier,[18,19] together with other transitions at λ_{max} = 440, 680 and 760 nm. The same spectral details were observed in the ns transient produced in the 355 nm excitation of the [$^2H_8$]naphthalene complex.

Owing to the persistence of $(NAPH)_2^{\bullet+}$ on the ns time-scale, the quantum yield Φ for its formation could be readily measured by the method of relative actinometry[20] based on the benzophenone triplet (λ_{max} = 530 nm)[21] as the transient actinometer, *i.e.*, $\Phi = \Phi_{BT}$ $(\varepsilon_{BT}/\varepsilon)(A/A_{BT})$, where Φ_{BT} is the quantum yield for the formation of benzophenone triplet (taken as 1.0), ε_{BT} and ε are the extinction coefficients of benzophenone triplet and $(NAPH)_2^{\bullet+}$, respectively,[22] and the ratio (A/A_{BT}) represents the 580 nm absorbance of $(NAPH)_2^{\bullet+}$ relative to the

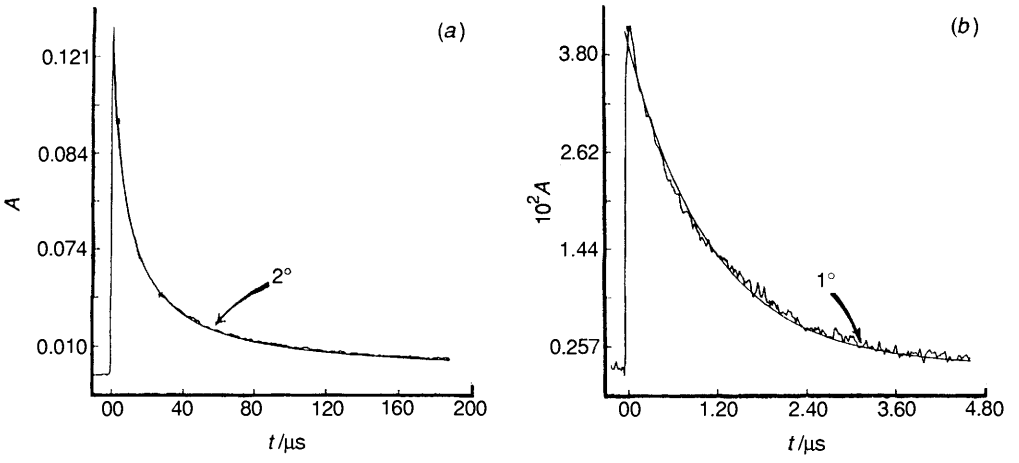

Fig. 5 (*a*) Spectral decay of $(NAPH)_2^{\bullet+}$ at 580 nm following the 355 nm excitation of $MeOPyNO_2^+$ and 0.2 mol dm^{-3} naphthalene in acetonitrile at 23 °C. The smooth curve is the computer-generated second-order fit. (*b*) Change in the decay profile to first-order kinetics in the presence of added (0.35 mmol dm^{-3}) NO_2.

Table 4 Second-order kinetics for the spectral decay of naphthalene cation radicals[a]

Nitrating agent	Naph. (mol dm^{-3})	A_i[b]	τ[c] μs	k_{II}[d] 10^6 A^{-1} s^{-1}
$MeOPyNO_2^+$	0.2 ($C_{10}H_8$)	0.15	8.5	0.75
		0.068	15	0.81
		0.013	69	1.1
$MeOPyNO_2^+$	0.2 ($C_{10}D_8$)	0.21	6.4	0.69
		0.080	15	0.80
		0.018	50	1.2
TNM	0.2 ($C_{10}H_8$)	0.12	7.0	0.78
		0.030	35	0.90

[a] Generated by CT excitation of the naphthalene complex with *N*-nitro-4-methoxypyridinium and tetranitromethane at 355 and 532 nm, respectively. [b] Initial (580 nm) absorbance at variable laser power. [c] Time for absorbance decrease to half A_i. [d] Measured second-order rate constant for $(NAPH)_2^{\bullet+}$ decay at 580 nm.

530 nm absorbance of benzophenone triplet. The value of Φ = 0.82 ± 0.05 was determined in the time interval: $10 < t < 100$ ns after the CT excitation of the naphthalene complex with *N*-nitro-4-methoxypyridinium in acetonitrile at 23 °C.

Temporal Evolution of Naphthalene Cation Radicals.—The subsequent disappearance of naphthalene cation radical was observed as the uniform decay of all the absorption bands in Fig. 4 (at the same rate) to the spectral baseline within 200 μs—to yield finally a residual spectrum with only a minor absorption at *ca.* 350 nm. The adherence of the absorbance change $(A_0 - A)$ at λ_{max} = 580 nm to second-order kinetics was clearly indicated by the precise fit of the computer-generated (smooth) line, as typically shown in Fig. 5(*a*). (Note the time interval for the least-squares treatment is bracketed by the pair of asterisks.) The second-order decay was also confirmed in Table 4 by (*a*) the constancy of the rate constant k_{II} = 0.8 ± 0.1 × 10^6 A^{-1} s^{-1} evaluated in this manner over a four-fold variation in the initial absorbance A_0 (proportioned to the laser power), as well as (*b*) the inverse variation of the apparent halflife (τ) with A_0.[23] The experimental second-order rate constant measured directly in absorbance units from the CT excitation of the naphthalene complex with *N*-nitro-4-methoxypyridinium was equivalent to the standard second-order rate constant k_{II} = 3.3 ± 0.5 × 10^9 dm^3 mol^{-1} s^{-1} when the extinction coefficient ε_{580} = 3600 dm^3 mol^{-1} cm^{-1} was used for the 580 nm absorbance of $(NAPH)_2^{\bullet+}$.[22] It is noteworthy that the analogous spectral decay from the 532 nm CT excitation of the corresponding tetranitromethane complex obeyed the same second-order kinetics—with the value of k_{II} = 3.0 ± 0.4 × 10^9 dm^3 mol^{-1} s^{-1} being experimentally indistinguishable from that evaluated for the nitropyridinium complex (see Table 4). In both cases, the stoichiometry for charge-transfer nitration in eqns. (6) and (8) allowed the spectral decay of naphthalene cation radicals to be assigned to the common reaction with NO_2. The accompanying spectral decay of the latter was not observed owing to the nondescript (diffuse) NO_2 absorption.[24,25]

The deuterium kinetic isotope effect on the disappearance of naphthalene cation radical was determined from the CT excitation of [$^2H_8$]naphthalene and *N*-nitro-4-methoxypyridinium. Under the reaction conditions described in Table 4, the second-order rate constants k_{obs} for $NAPH^{\bullet+}$ and [$^2H_8$]$NAPH^{\bullet+}$ were found to be the same within the experimental uncertainty.

The effects of nitrogen dioxide and pyridine on the spectral decay of naphthalene cation radical were most conveniently studied with 532 nm excitation by using tetranitromethane as the acceptor, since this EDA complex was insensitive to the presence of such additives. (The alternative use of the 355 nm excitation to generate the naphthalene cation radical from the nitropyridinium complex was also discouraged by the strong absorption of the laser pulse by the dimeric N_2O_4.[26])

(*a*) *Nitrogen dioxide* was vacuum transferred into a dual-compartmented photochemical/electrochemical cell of local design[27] that contained the predetermined amounts of naphthalene and tetranitromethane in acetonitrile solution. The concentration of dissolved nitrogen dioxide was measured *in situ* by linear-sweep voltammetry using a platinum microelectrode (see the Experimental section for the details of the analysis). Under these conditions, the spectral decay of naphthalene cation radical obeyed first-order kinetics to beyond four halflives [see Fig. 5(*b*)]. The rate constant k_1 followed a pseudo-first-order dependence on the concentration of nitrogen dioxide [NO_2], as illustrated in Fig. 6(*a*), and the overall second-order rate constant (k_{II}) evaluated from the slope is also listed in Table 5.

(*b*) *Pyridine* was typically added in incremental amounts to a photochemical cell that contained naphthalene and tetranitromethane dissolved in acetonitrile. Attendant upon the 532 nm excitation of the EDA complex, the spectral decay of naphthalene cation radical followed clean first-order kinetics to beyond four halflives. Fig. 6(*b*) shows the linear dependence of the rate constant k_1 on the concentration of added pyridine, and the second-order rate constant (k_{II}) is also listed in Table 5. The same kinetic behaviour was observed with added 2,6-lutidine, but with a significantly reduced slope. Moreover, the decay rate

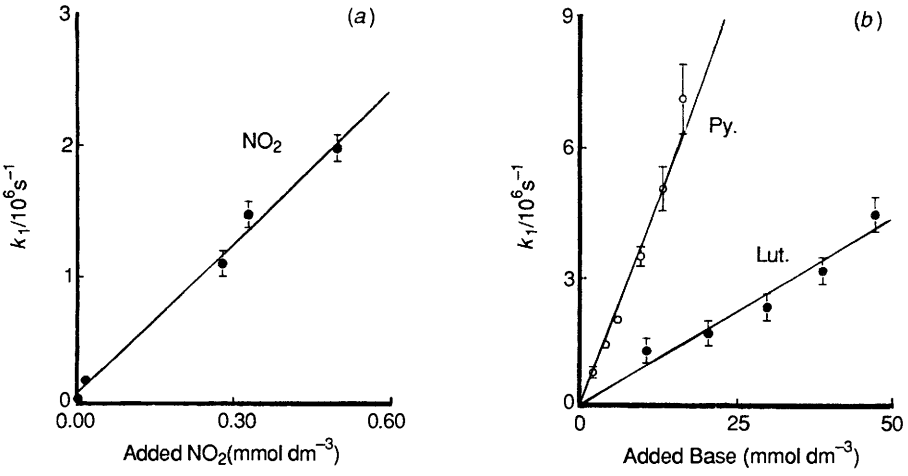

Fig. 6 Pseudo-first-order plots for the spectral decay of $(NAPH)_2^{\bullet+}$ at 580 nm in the presence of (*a*) NO_2 and (*b*) various pyridines, as indicated

Table 5 Effects of added nitrogen dioxide and various pyridines on the spectral decay of naphthalene cation radicals[a]

Additive	*c* / mmol dm^{-3}	k_1[b] / 10^3 s^{-1}	k_{II}[c] / dm^3 mol^{-1} s^{-1}	Additive	*c* / mmol dm^{-3}	k_1[b] / 10^6 s^{-1}	k_{II}[c] / dm^3 mol^{-1} s^{-1}
NO_2	0.015	0.18		2,6-Lutidine	4.2	0.75	
	0.28	1.1			10	1.3	
	0.33	1.5			20	1.7	
	0.50	2.0	4.0×10^9		30	2.3	
					39	3.2	
					48	4.5	8.0×10^7
Pyridine	2.0	0.75		2,6-$(Bu^t)_2$-4-MePy	5.8	0.42[d]	
	4.0	1.4			11	0.54[d]	
	5.9	2.0			16	0.67[d]	
	9.5	3.5			26	0.75[d]	
	13	5.1			35	0.90[d]	
	16	7.1	3.8×10^8		43	0.95[d]	$<2 \times 10^7$

[a] $(NAPH)_2^{\bullet+}$ generated by 532 nm excitation of 0.2 mol dm^{-3} naphthalene and 0.6 mol dm^{-3} TNM in acetonitrile at 23 °C. [b] Pseudo-first-order rate constant. [c] Second-order rate constant. [d] Treated as first-order decay (see the text).

Table 6 Common-ion effect on the decay kinetics of naphthalene cation radicals[a]

TNM / (mol dm^{-3})	Naph. / mol dm^{-3}	TBA^+T^- / mol dm^{-3}	k_{II}[b] / 10^6 A^{-1} s^{-1}
0.3	0.1	0	4.0
		0.032	5.2
		0.10	7.0
		0.18	4.5
		0.26	6.5
0.7	0.2	0	3.2
		0.07	7.2
		0.14	8.4
		0.26	6.4

[a] $(NAPH)_2^{\bullet+}$ generated by 532 nm excitation of the EDA complex in acetonitrile at 23 °C. [b] Second-order rate constant for spectral decay at λ = 580 nm.

was almost invariant with the highly hindered 2,6-di-*tert*-butyl-4-methylpyridine as the added base (see Table 5).

In the charge-transfer nitration of naphthalene with tetranitromethane, one equiv. of nitroform was formed according to the stoichiometry in eqn. (6). Since it is extensively ionized in acetonitrile,[15b] trinitromethanide as the tetra-*n*-butylammonium salt (TBA^+T^-) was added in the amounts listed in Table 6 to the acetonitrile solution of the EDA complex prior to irradiation. In all cases, the disappearance of naphthalene cation radical was essentially unaffected by the presence of trinitromethanide—the spectral decay following second-order kinetics over the entire range of added salt.

Discussion

The nitration of naphthalene with various *N*-nitropyridinium cations X–$PyNO_2^+$ affords essentially the same mixture of α- and β-nitronaphthalenes according to the stoichiometry in eqns. (4) and (5), irrespective of whether the substitution is effected under the electrophilic (thermal) or the charge-transfer (photochemical) conditions presented in Tables 1 and 2. Thus any (slight) compositional variation of α- and β-isomers within the experimental limits of (92 ± 6)% and (8 ± 6)%, respectively is, by itself, insufficient to distinguish the electrophilic from the charge-transfer pathway, the preponderant nitration of naphthalene at the α-position being the consistent result. [At this juncture, we re-emphasize the caveat[3] that any *small* change in the yield of the minor β-isomer is grossly magnified in the value of the α/β ratio; and thus the direct comparison of absolute (isomer) yields, and not their ratio, is a more useful diagnostic guide.] Particularly noteworthy is the fact that the nature of the nitrating agent, be it *N*-nitropyridinium with various X-substituents, tetranitromethane or nitric acid/acetic anhydride, plays no or little role in affecting the selectivity in naphthalene nitration. Consequently, it is reasonable to conclude that (*a*) the initial transfer of the NO_2 group from the

Table 7 Second-order rate constants for reaction of naphthalene cation radicals

Additive	k_{II}[a] / $dm^3\ mol^{-1}\ s^{-1}$	k_2[b] / $dm^3\ mol^{-1}\ s^{-1}$
NO_2	4×10^9	2×10^{11}
Pyridine	4×10^8	2×10^{10}
2,6-Lutidine	8×10^7	5×10^9
2,6-Di-*tert*-butyl-4-methylpyridine	2×10^7	1×10^9

[a] Observed second-order rate constant for $(NAPH)_2^{\bullet+}$ decay in the presence of additive. [b] Calculated rate constant for $NAPH^{\bullet+}$ (see the Appendix).

nitrating agent ($Y-NO_2$) to naphthalene is a step common to both electrophilic and charge-transfer nitration, and (*b*) the nucleofugal group Y = pyridine, trinitromethanide, acetate, *etc.* is involved only after the isomeric (α/β) substitution pattern is established.

Charge-transfer Activation of Naphthalene.—In order to focus on the sequential transformations qualitatively outlined above, let us consider how the time-resolved spectroscopy of naphthalene cation radicals in Fig. 4 can be used to delineate their role as the prime reactive intermediates in charge-transfer nitration. Thus the high quantum yield of $\Phi = 0.8$ for the formation of naphthalene cation radicals accords with the efficient activation of the EDA complex by the charge-transfer mechanism delineated in earlier studies,[3,13] Scheme 2, where Y =

$$NAPH + YNO_2^+ \overset{K}{\rightleftharpoons} [NAPH, YNO_2^+] \quad (11)$$

$$[NAPH, YNO_2^+] \overset{h\nu_{CT}}{\rightleftharpoons} [NAPH^{\bullet+}, Y, NO_2] \quad (12)$$

$$[NAPH^{\bullet+}, Y, NO_2] + NAPH \xrightarrow[fast]{} (NAPH)_2^{\bullet+} + Y + NO_2 \quad (13)$$

Scheme 2

pyridine, trinitromethanide,[15] *etc.* Furthermore, the (picosecond) evolution of the naphthalene cation radical to the dimer cation radical (Fig. 3) indicates that the bimolecular π-association in eqn. (13) is to be included amongst the earliest temporal events.[13]

Homolytic Collapse of Naphthalene Cation Radicals to the Wheland Intermediate.—Although the reactivities of the aromatic cation radical and their π-dimers differ,[28] let us initially focus on the fate of $NAPH^{\bullet+}$ arising from the facile dissociation in eqn. (10). Thus the observation of second-order kinetics (k_2) for the spectral decay in Fig. 5(*a*) (see Table 4) points to the disappearance of freely diffusing $NAPH^{\bullet+}$ after its separation from the initially-formed triad in eqn. (12). Owing to the high yields of the nitronaphthalenes observed (see Table 2), such a process can be readily formulated as the bimolecular (homolytic) reaction that produces the critical Wheland intermediate,[4–6] *i.e.*, Scheme 3.*

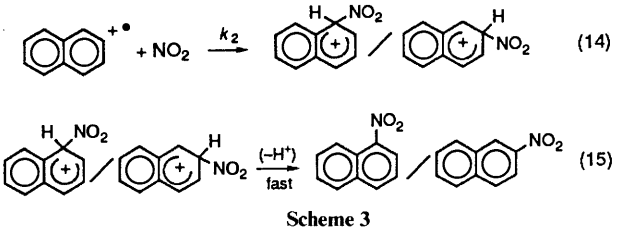

Scheme 3

* The base for deprotonation in eqn. (15) can be the solvent (acetonitrile) and/or Y = pyridine, *etc.* (*vide infra*).

According to Scheme 3, the isomeric product ratios are established during the collapse of the radical pair [eqn. (14)], consonant with the invariant α/β values in Table 2 (column 8) despite any marked changes in either the reactivity or the steric bulk of the various nitrating agents $X-PyNO_2^+$, $C(NO_2)_4$, *etc.* Furthermore, the absence of a measurable deuterium kinetic isotope effect in the decay of $[^2H_8]NAPH^{\bullet+}$ (Table 4) is predicted from Scheme 3, since the proton loss occurs in a fast subsequent step [eqn. (15)].[15b,29] {The absence of a deuterium kinetic isotope effect also indicates that the presence of pyridine in the triad [eqn. (12)] does not lead to the nitronaphthalenes by an alternative pathway involving the prior deprotonation of the naphthalene cation radical followed by a free-radical coupling with NO_2.}

The time-resolved spectroscopic study on the picosecond timescale (Fig. 2) establishes that the steady-state concentration of naphthalene cation radicals consists primarily of the dimeric form [see eqn. (10)]. In order to determine whether the subsequent reaction with NO_2, as given in Scheme 3, is quantitatively consistent with the observed second-order kinetics in Table 4, let us separately evaluate the reversible dissociation in eqn. (16). Extrapolation of the low-temperature

$$NAPH^{\bullet+} + NAPH \underset{k_d}{\overset{k_a}{\rightleftharpoons}} (NAPH)_2^{\bullet+} \quad (16)$$

data[19] yields a formation constant $K = k_a/k_d$ of *ca.* 300 $dm^3\ mol^{-1}$ at 23 °C. This value, coupled with the association rate constant (k_a) of *ca.* $10^{10}\ dm^3\ mol^{-1}\ s^{-1}$ in Fig. 3, yields an estimate of the dissociation rate constant (k_d) of *ca.* $10^8\ s^{-1}$. The application of the usual (pseudo) steady-state constraints to the disappearance of $NAPH^{\bullet+}$ [based on the combination of eqns. (16) and (14)], yields the calculated values of k_2 in Table 7 (see the Appendix). For convenience, the experimental second-order rate constants k_{II} [determined from either the second-order decays in Fig. 5(*a*) or the pseudo first-order treatment in Fig. 5(*b*)] are also included in Table 7. Although the calculated values of the second-order rate constants of $NAPH^{\bullet+}$ with the various pyridines are reasonable, the magnitude of k_2 for reaction with NO_2 exceeds the (estimated) diffusion-limited rate constant of *ca.* $2 \times 10^{10}\ dm^3\ mol^{-1}\ s^{-1}$.[27] The latter suggests a contribution from $(NAPH)_2^{\bullet+}$ in the NO_2 reaction described in Scheme 3. However, this slight ambiguity does not materially affect the mechanistic formulation, since the naphthalene cation radical as a *planar* moiety is subject to the same steric access by NO_2 irrespective of whether it is shielded on one face, the loose naphthalene association extant in $(NAPH)_2^{\bullet+}$ being insufficient[30] to differentiate the Wheland intermediates from those derived *via* $NAPH^{\bullet+}$.

Annihilation of the Wheland Intermediate: Competition between Naphthalene Nitration and Adduct Formation.—The importance of the nitro-pyridine adduct **B** (and isomers) as by-products of the charge-transfer nitration in Table 3 is directly related to the reactivity and availability of pyridine, particularly as a nucleophile. Thus, little or no adducts are produced when the pyridine moiety (X–Py) consists of either the highly hindered 2,6-lutidine[31] with a pair of *ortho* methyl groups (entry 1) or the weak base 4-methoxycarbonylpyridine[32] with the strongly electron-withdrawing (CO_2Me) substituent with Hammett $\sigma = 0.45$[33] (entry 2). Moreover, the 4-methoxypyridine adducts formed in modest yields (entry 3, Table 2) are singularly unimportant when the charge-transfer nitration is carried out in the presence of trifluoroacetic acid (entry 5) to intercept any free MeOPy.

The appearance of the naphthalene adduct **B** (and its isomers) during charge-transfer nitration is readily reconciled with the Wheland intermediate in Scheme 3 when the dual role of pyridine as base [eqn. (17)] and as nucleophile [eqn. (18)] is

considered, Scheme 4. According to Scheme 4, adducts are

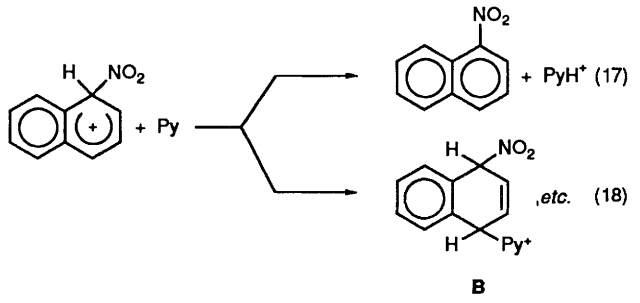

Scheme 4

formed in competition with nitration, and they are disfavoured by sterically encumbered bases (*e.g.* 2,6-lutidine) or weak nucleophiles (*e.g.* 4-methoxycarbonylpyridine) which hinder the cation neutralization [eqn. (18)] relative to deprotonation.[15c,34]

The alternative pathway for adduct formation involving an initial (nucleophilic) addition of the pyridine to the naphthalene cation radical, followed by NO_2 coupling, is ruled out by the kinetic results in Table 5, in which the second-order rate constant for reaction of naphthalene cation radical with NO_2 [eqn (14)] is shown to be an order of magnitude faster than that with pyridine. The same kinetics argument applies to the formation of the naphthalene adduct **C** (and its isomers) from tetranitromethane, Scheme 5.

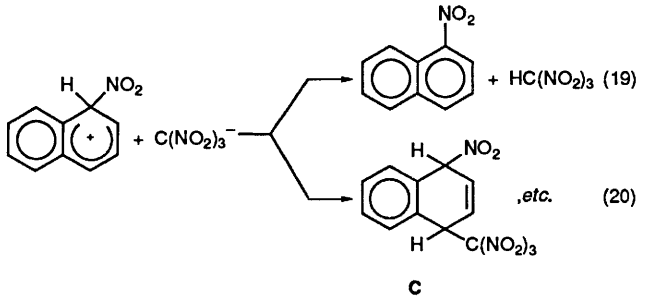

Scheme 5

For this nitration system, the rate constants in Table 6 show that the nucleophilic addition of trinitromethanide to naphthalene cation radical is at least three orders of magnitude too slow to compete effectively with the formation of the Wheland intermediates in eqn. (14). Indeed, the relatively high yields of adduct **C** from TNM (compared with the yields of adduct **B** from $MeOPyNO_2^+$) can be readily accounted for by the signficantly lower base strength of trinitromethanide ($pK_B \sim 14$)[35] relative to 4-methoxypyridine ($pK_B = 7.4$)[32] for the competitive deprotonation of the Wheland intermediates in Schemes 4 and 5. Moreover, the step leading to the formation of the trinitromethanide adduct **C** (and isomers) in eqn. (20) corresponds to a facile annihilation of ion pairs, which has previously been delineated in a similar system.[36,37]

The Common Mechanism for Charge-transfer Nitrations with N-Nitropyridinium and Tetranitromethane.—The pair of the cationic Wheland intermediates in Scheme 3 resulting from NO_2 addition at the α- and β-positions of the naphthalene cation radical will be neutralized by either pyridine or trinitromethanide to afford two series of adducts in which the nitro substituent is situated on either an α- or β-position.[38] Although these are partially identified in the complex ^1H NMR spectra of the adduct mixtures (see the Experimental section), only a single isomer **C** has been successfully isolated and structurally characterized. Nonetheless, we suggest that the

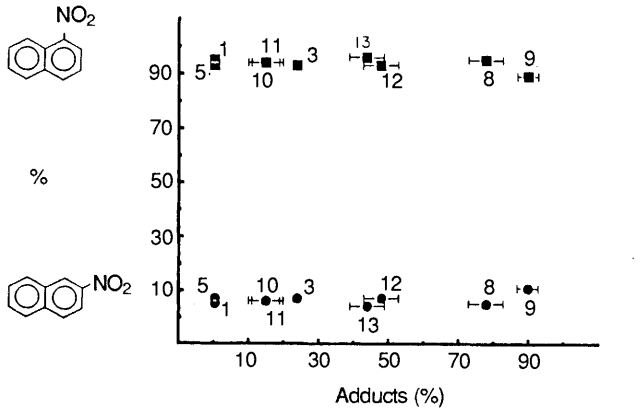

Fig. 7 Isomeric mixtures of α-nitronaphthalene (■) and β-nitronaphthalene (●) produced in competition with naphthalene adducts (**B**, **C**, *etc.*) under various conditions for naphthalene nitration with both $X-PyNO_2^+$ and TNM acceptors, as identified in Table 3 (by entry numbers) together with (11) $MeOPyNO_2^+$ plus 2 equiv. CF_3CO_2H in acetonitrile, (12) TNM plus 2 equiv. CF_3CO_2H in chloroform, and (13) TNM plus 2 equiv. CF_3CO_2H in acetonitrile

overall isomeric composition of the α/β-adduct mixture can be deduced from the unique behaviour of adduct **C**. For example, the conversion of a crystalline sample of **C** in acetonitrile to only a single product (α-nitronaphthalene) upon aqueous or hydrogencarbonate treatment [see eqn. (7)], indicates that the hydrolytic elimination of $H-C(NO_2)_3$ is regiospecific. Since such an aromatization is likely to occur by either an E_2 or E_1CB process in aqueous acetonitrile, similar regiospecificity should apply to the other isomeric adducts. Thus the observation (Table 2) that α- and β-nitronaphthalenes are formed during charge-transfer nitration with essentially the same isomeric ratio as that derived in Table 3 by the subsequent (separate) hydrolytic elimination of the adduct mixture [eqn. (9)], supports the partitioning of the Wheland intermediate as a common mechanism (Schemes 4 and 5) that is equally applicable to such structurally distinct nitrating agents as *N*-nitropyridinium and tetranitromethane.

Since the isomeric composition is established in the prior step involving the attack of NO_2 on naphthalene cation radical (see Scheme 3), it follows that the relative amounts of α-and β-nitronaphthalene will be independent of the nitrating agent $Y-NO_2$, as evaluated by the base/nucleophilic strength of the nucleofugal group [Y = X-Py, $C(NO_2)_3^-$, *etc.*].* This prediction is borne out by the experimental results presented in Fig. 7. In the context of Schemes 3–5, such a striking result indicates that the partitioning of the α/β-Wheland intermediates is quite independent of the fraction trapped (by pyridine and trinitromethanide) to afford the adducts **B** and **C** (plus isomers). Thus in the nitration of naphthalene, the adduct formation represents an extraneous side reaction that does not directly impinge on the isomeric distribution of the nitronaphthalenes, its importance being largely an independent function of the nucleophilic reactivity and concentration of Y = pyridine, trinitromethanide, *etc.* The latter is indeed consistent with the lower adduct yield that is obtained in charge-transfer nitration when the incident light flux is deliberately attenuated (compare entries Nos. 3 and 6 in Table 3). Thus it can be shown that the steady-state concentration of pyridine in charge-transfer nitration with $PyNO_2^+$ can be simply expressed as eqn. (21),

$$^{CT}[Py]_{ss} = (I_0/k_2)^{\ddagger} \quad (21)$$

where I_0 is the incident light flux per unit volume of photolysate

* Implicit in this conclusion is that the reversibility of NO_2 addition is slower than deprotonation/adduct formation.

expressed in einstein dm^{-3} s^{-1} and k_2 is the second-order rate constant in eqn. (14) (Scheme 3).[39]

Relevance of the Charge-transfer Mechanism to the Electrophilic Nitration of Naphthalene.—Electrophilic and charge-transfer nitrations of naphthalene (NAPH) with *N*-nitropyridinium ($X\text{-}PyNO_2^+$) share in common the rapid, pre-equilibrium formation of the metastable EDA complex [NAPH, $X\text{-}PyNO_2^+$] in eqn. (1). Moreover, the subsequent activations of these EDA complexes to yield indistinguishable mixtures of α/β nitronaphthalenes in Tables 1 and 2 suggest that the same, or closely related, reactive intermediates are involved in both processes. Since time-resolved spectroscopy establishes naphthalene cation radicals and NO_2 as the critical intermediates in charge-transfer nitration according to Scheme 2, the most direct formulation of the electrophilic process invokes the production of the same intermediates *via* a *thermal* process, *e.g.* Scheme 6. Since such an electron transfer represents the

$$NAPH + X\text{-}PyNO_2 \overset{K_{EDA}}{\rightleftharpoons} [NAPH, X\text{-}PyNO_2^+] \quad (22)$$

$$[NAPH, X\text{-}PyNO_2^+] \xrightarrow{k_E} NAPH^{\bullet+}, X\text{-}Py, NO_2 \quad (23)$$

Scheme 6

adiabatic counterpart to the photochemical process, the triad in eqn. (23) is (stoichiometrically) equivalent to that in eqn. (12) and its collapse to the Wheland intermediates would lead to the same mixture of isomeric nitronaphthalenes as described in Scheme 3. Indeed, the participation of naphthalene cation radicals in electrophilic nitration, as presented in Scheme 6, accords with the elegant CIDNP studies of aromatic nitration with nitronium ion, *e.g.* by Ridd, Sandall and coworkers.[40] Since the predicted rate of electron transfer (k_E) for eqn. (24),

$$NAPH + NO_2^+ \xrightarrow{k_E} NAPH^{\bullet+} + NO_2, \textit{etc.} \quad (24)$$

based on *outer-sphere* Marcus theory and E° and λ for $NAPH/NAPH^{\bullet+}$ and NO_2^+/NO_2, is too slow,[41] the possibility of an inner-sphere mechanism for electron transfer must be contemplated.[10] Indeed, an inner-sphere activated complex [NAPH, NO_2^+] ⟷ [$NAPH^{\bullet+}$, NO_2] consisting of a bent O–N–O moiety could accommodate the kinetics restriction,[42] and it has a structural analogy in the inner-sphere complexes of aromatic donors with nitrosonium ion which have been established by X-ray crystallography.[43]

Electron-transfer energetics pose an even greater (kinetics) restriction for the *N*-nitropyridinium electrophile, at first glance, since its reduction (which is electrochemically irreversible) occurs at potentials of roughly a volt more negative than that for NO_2^+.[44] Ambiguity in the reversible reduction potential

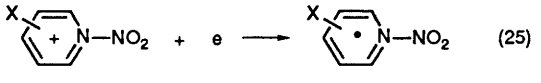

(25)

(E°) arises from the very short lifetime of the *N*-nitropyridinyl radical,[45] and there is a question as to whether it is even a bound state. The latter suggests the possibility that the adiabatic electron transfer to *N*-nitropyridinium occurs with the simultaneous cleavage of the $N\text{–}NO_2$ bond, eqn. (26), which

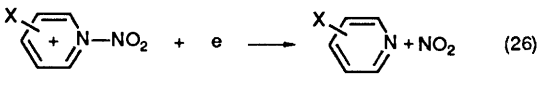

(26)

is implicit in eqn. (23). Unfortunately, a predictive (kinetics) model for such a dissociative electron attachment to $X\text{-}PyNO_2^+$ from an aromatic donor is unavailable, especially in view of the uncertain intermolecular separations among $NAPH^{\bullet+}$, Py and NO_2 in eqn. (23). The latter is directed to the parallel point that the thermal (adiabatic) triad resembles the (photochemical) triad in eqn. (12) to the degree that the nitropyridinyl radical produced during the vertical (charge-transfer) excitation of the EDA complex suffers spontaneous fragmentation to Py and NO_2. If so, the subsequent steps outlined in Schemes 3 and 4 should be the same for the electrophilic and charge-transfer processes, especially with regard to the branching of the Wheland intermediate to nitronaphthalenes and adducts. Let us consider therefore how the mechanism in Scheme 6 actually predicts the small role that the naphthalene adducts generally play in electrophilic nitration in comparison with charge-transfer nitration—despite the common role of the triad in both processes.

From Scheme 4, we recognize the critical importance of nucleophile availability for the formation of adduct. Accordingly, the steady-state concentration of pyridine in electrophilic nitration with $PyNO_2^+$ can be derived from Scheme 6 as the relationship[39] given in eqn. (27), where R_E is the rate of eqn.

$$^{E}[Py]_{ss} = (R_E/k_2)^{\frac{1}{2}} \quad (27)$$

(23)[46] expressed in mol dm^{-3} s^{-1} and k_2 is the second-order rate constant in eqn. (14) (Scheme 3). Since the latter is taken to be the same in eqns. (21) and (27), it drops out in the comparative steady-state concentrations, *i.e.*, eqn. (28). Taking reasonable

$$^{CT}[Py]_{ss}/^{E}[Py]_{ss} = (I_0/R_E)^{\frac{1}{2}} \quad (28)$$

estimates of $I_0 = 10^{-1}$ einstein dm^{-3} s^{-1} and $R_E = 10^{-5}$ mol dm^{-3} s^{-1}, we conclude that the steady-state concentration of pyridine is indeed *ca.* 100 times greater than that extant during electrophilic nitration.* This important conclusion will be more fully elaborated later[39] in the direct comparison of electrophilic and charge-transfer nitration of 1,4-dimethylnaphthalene, since the dominant adduct formation can be more accurately and reliably assessed with this aromatic substrate.[13]

Experimental

Materials.—Naphthalene (Aldrich) was recrystallized from absolute ethanol and dried *in vacuo*. Crystalline $4\text{-}X\text{-}PyNO_2^+\text{-}BF_4^-$ salts were prepared from pure $NO_2^+BF_4^-$ (and the appropriate pyridine) to avoid contamination by nitrosonium impurity as described previously.[2] *N*-Nitro-2,6-lutidinium tetrafluoroborate was similarly synthesized at −20 °C from $NO_2^+BF_4^-$ and 2,6-lutidine in acetonitrile. Recrystallization from a mixture of acetonitrile and ethyl ether at −20 °C yielded the colourless crystalline salt: δ(CD_3CN) 2.91 (s, 6 H), 7.95 (d, 2 H) and 8.50 (t, 1 H); $\nu_{max}(CD_3CN)/cm^{-1}$ 3210, 3140, 3110, 3010, 2920, 2860, 1739, 1670 (asymmetric NO_2 stretch), 1650, 1630, 1565, 1550, 1430, 1310, 1280, 1260, 1175, 1100 ~ 1070 (BF_4^-), 930, 795, 558 and 520. Authentic samples of α- and β-nitronaphthalene were obtained commercially (Aldrich), and used as comparative standards for analysis. Pyridine (Mallinckrodt) and 2,6-lutidine (Mattheson, Coleman and Bell) were redistilled from calcium hydride and stored under an

* The minor amounts of naphthalene adducts (**B**, *etc.*) that may be formed during electrophilic nitration with $X\text{-}PyNO_2^+$ under neutral conditions would also largely reflect the α/β-Wheland intermediates, as described in Section 4. However, this may not be true of the adducts formed in electrophilic nitration as usually carried out (HNO_3, HNO_3–H_2SO_4, *etc.*) since acid-catalysis in the latter case would probably lead to (partial) equilibration of α/β-Wheland intermediates.

argon atmosphere. 2,6-Di-*tert*-butyl-4-methylpyridine (Aldrich) was sublimed *in vacuo* and stored in a dry box until used. Tetranitromethane was prepared in the earlier study.[3]

Acetonitrile (Fisher) was stirred with $KMnO_4$ for 24 h and the mixture was refluxed until the liquid was colourless. After removal of the brown MnO_2 by filtration the acetonitrile was distilled from P_2O_5 under an argon atmosphere. Acetonitrile was again fractionated from CaH_2 and stored in a Schlenk flask under an argon atmosphere. Dichloromethane (J. T. Baker) was initially stirred with concentrated sulfuric acid. The separated layer was neutralized and dried over anhydrous Na_2CO_3. It was finally distilled from anhydrous P_2O_5 under an argon atmosphere. Trifluoroacetic acid (Mallinckrodt) was refluxed with and then distilled from P_2O_5.

Instrumentation and Analysis.—The UV–VIS absorption spectra were measured on a Hewlett-Packard model 8450A diode array spectrometer equipped with an HP 89100A temperature controller. The ^1H NMR spectra were recorded on a JEOL FX 90Q spectrometer operating at 90 MHz, and the proton chemical shifts are reported in ppm downfield from a tetramethylsilane internal standard. IR spectra were obtained with an AgCl cell by using a Nicolet 10DX FT spectrometer with 4 cm^{-1} resolution.

GC analyses were performed on a Hewlett-Packard 5790A chromatograph equipped with a flame ionization detector, using a 12.5 m SE-30 capillary column. For quantitative analyses, decane (Aldrich) was used as a calibration standard. High-performance liquid chromatography (HPLC) employed an LDC Analytical model 3000 equipped with dual pumps (constaMetric 3200 and 3500 solvent delivery systems) and an UV detector (spectroMonitor 3100). Analytical HPLC was carried out with a reversed-phase column (Hypersil BDS C_{18}, 5 μ). The mobile-phase solvents were 5% methanolic water (distilled) in solvent A and HPLC grade acetonitrile in solvent B. Integration of the signals was performed by a Hewlett-Packard HP3394A integrator. Naphthalene and the isomeric nitronaphthalenes were analysed by using a mixture of 40% solvent A and 60% solvent B with a flow rate of 1 cm^3 min^{-1} at 264 nm detection and quantified by integration method using *tert*-butylbenzene as an internal standard; compound, retention time and calibration factor in acetonitrile solution were naphthalene, 10.5, 39 ± 1; 1-nitronaphthalene, 8.0, 34 ± 1; 2-nitronaphthalene, 8.7, 113 ± 2; *tert*-butylbenzene, 18.3, 1.00. Such quantification of the products was always accompanied by GC analyses. Both GC and HPLC analysis consistently afforded identical results within the experimental error limits. All manipulations of the moisture-sensitive *N*-nitropyridinium salts were carried out in a Vacuum Atmospheres HE-439 dry box maintained at <2 ppm water.

The light source for charge-transfer nitration consisted of a 500 W Osram HB mercury lamp equipped with a parabolic reflector. The light was passed through a circulating water filter to remove IR radiation, and a fused silica biconvex lens (φ = 4.5 cm, f = 10 cm) focused the light onto the sample contained in 1.0 cm quartz cuvette. (For diffuse irradiations, the focusing lens was removed and a 10 cm cuvette was used.) A sharp cut-off filter (Corning CS-3 series, No. 3060, 3391, 3387, 3385 and 3384 for λ_{exc} > 380, 410, 425, 480 and 500 nm, respectively) was fixed in front of the cell to ensure that only the charge-transfer band of the relevant EDA complex was irradiated. Temperature control was achieved by immersing the sample cuvette in a stirred acetone bath that was contained in a Pyrex dewar and cooled automatically in the temperature range from −60 to −40 ± 2 °C with the aid of a Neslab CC-65A immersion chiller. The dark control was always carried out simultaneously in a light-tight cuvette.

The time-resolved differential absorption spectra on the picosecond timescale were obtained with a laser-flash system that utilized the 532 nm (second harmonic) and 355 nm (third harmonic) 20 ps pulses from a Quantel YG501-C mode-locked Nd:YAG laser as the excitation sources. The excitation beam was focused onto the sample with a cylindrical (fused silica) lens (f2). The analysing beam was produced by focusing the residual fundamental (1064 nm) on a mixture (1:1 v:v) of H_2O and D_2O contained in a 10 cm cuvette. The white light produced (400–800 nm) was focused onto a bifurcated fibre bundle (Dolan Jenner) which directed the two analysing beams through the excited and unexcited volumes of the sample at a 90° angle to the excitation beam. The analysing beams passed through the sample and were collected by a fibre optic cable that was connected to a monochromator (ISA HR320). The signal was recorded on a dual diode array (Princeton Instruments DD512) that was calibrated with the 436 and 542 nm lines from a mercury lamp. Time resolution was achieved by passing the fundamental (1064 nm) along a delay stage (Velmex B4036Q13) to vary the pathlength of the probe light with respect to the excitation beam. The time-resolved spectral studies on the nanosecond/microsecond timescales were carried out with a spectrometer consisting of Quantel YG580-10 Q-switched Nd-YAG laser with a pulsewidth of 10 ns. The second (532 nm) and third (355 nm) harmonic were used for excitation. The excitation energy was attenuated with various copper-wire mesh filters that were placed in the beam path. The probe beam consisted of the output from a 150 W xenon arc lamp mounted in an Oriel housing that was equipped with an Aspherlab UV-grade condensing lens. The probe beam was focused onto the sample, and the merging beam from the sample was focused onto the entrance slit of an Oriel 77250 monochromator. Depending on the spectral region studied, the following gratings were used: Oriel 77299, 1-micron blaze, 600 line per mm for the 600–1050 region and Oriel 77298, 500 nm blaze, 1200 lines per mm for the 300–1000 nm region. The detector housing was attached to the exit slit of the monochromator. Either a Hamamatsu (R928 photomultiplier tube (for the 200–800 nm region) or a Hamamatsu R406 photomultiplier tube (for the 600–1050 nm region) was used as the detector. A Kinetic Instruments lamp pulser was used to trigger the xenon lamp to produce sufficient light intensity in the near IR region. The timing sequence of the excitation and the probing of the sample were controlled by a Kinetic Instruments sequence-generator and laser-controller. Data acquisition and digitization were performed with a Tektronix 7104 oscilloscope in conjunction with a Tektronix C101 video camera and Tektronix DC501 software.

Electrophilic Nitration of Naphthalene with N-*Nitropyridinium Salts.*—The electrophilic nitration of naphthalene (0.045 mmol) was carried out with $PyNO_2^+BF_4^-$ (0.025 mmol) in acetonitrile or [$^2H_3$]acetonitrile under an argon atmosphere. No thermal reaction was apparent at −40 °C, as shown by an invariant charge-transfer spectrum over the course of 10 h. As the solution was warmed, the progress of nitration was spectrally followed by changes in the CT band and by ^1H NMR analysis of PyH^+, naphthalene and α/β-nitronaphthalene. The addition of diethyl ether, followed by filtration of the colourless pyridinium salts, afforded a nitronaphthalene solution which was quantitatively analysed by HPLC and GC-MS. The other nitropyridinium salts with X = 4-methoxy and 2,6-dimethyl (in 0.4 cm^3 CH_3CN) and 4-methoxycarbonyl (in 2.0 cm^3 CH_3CN) were treated similarly, and the results listed in Table 1.

Charge-transfer Nitration of Naphthalene with N-*Nitropyridinium Salts.*—Naphthalene (0.085 mmol) was added to 0.4 cm^3 of an acetonitrile solution of 0.082 mmol of *N*-nitro-4-methoxypyridinium salt under an argon atmosphere. Since the

yellow solution was unchanged for prolonged periods, it was deliberately irradiated with $\lambda_{exc} > 425$ nm at 23 °C. After 7 h, ^{1}H NMR analysis of the photolysate indicated α/β-nitronaphthalene, $MeOPyH^+$ (0.048 mmol), $MeOPyNO_2^+$ (0.032 mmol) and adducts [0.010 mmol, based on δ 6.38 (m) and 6.61 (m) for 4 H] and the photolysate was then divided equally. Diethyl ether was added to the first portion, and the pyridinium salts were removed by filtration. The resulting solution was diluted with pentane, washed with water and analysed by HPLC and GC. The other portion was found to be essentially unchanged (by ^{1}H NMR analysis), even after it was allowed to stand for a day.

The charge-transfer nitration of naphthalene (0.090 mmol) with 0.043 mmol of *N*-nitro-2,6-lutidinium salt in 0.4 cm^3 of CH_3CN was carried out at −40 °C with $\lambda_{exc} > 410$ nm. After 16 h, ^{1}H NMR analysis at −40 °C indicated 2,6-LuH^+ (*ca.* 0.04 mmol), unchanged $LuNO_2^+$ (0.005 mmol) and α/β-nitronaphthalene, together with minor olefinic resonances at δ 5.77 and 6.59 (<0.001 mmol). Addition of cold ether (−40 °C) led to the precipitation of the lutidinium salts; and the mother liquor was carefully decanted, washed with ice–water and immediately subjected to HPLC analysis (Table 2). Similar results were obtained with *N*-nitro-4-methoxycarbonylpyridinium tetrafluoroborate in 2 cm^3 of CH_3CN at −40 °C with $\lambda_{exc} > 500$ nm. The charge-transfer nitration of naphthalene was also carried out with *N*-nitropyridinium salt at −40 °C with $\lambda_{exc} > 425$ nm. After 10 h, ^{1}H NMR analysis indicated that most of the $PyNO_2^+$ had been consumed to produce PyH^+, (α/β)-nitronaphthalene and adducts (0.01 mmol based on δ 6.54, 6.58 and 6.60 for 4 H). Half of the photolysate was treated with pre-cooled diethyl ether at −40 °C and the pale yellow precipitate was removed by filtration. The HPLC analysis of the filtrate is given in Table 2. The other portion was allowed to warm to room temperature, and ^{1}H NMR analysis indicated that adduct persisted for at least an hour. However, upon standing for 12 h at 23 °C, *ca.* 50% of the adduct decomposed to a mixture of α/β-nitronaphthalenes.

Charge-transfer Nitration of Naphthalene with Tetranitromethane.—The red-orange solution of naphthalene (2.0 mmol) and tetranitromethane (TNM, 4 mmol) in 4 cm^3 of dichloromethane was bleached upon exposure to $\lambda_{exc} > 425$ nm at 23 °C. After 24 h, the photolysate was evaporated *in vacuo* and the residue dissolved in deuteriochloroform. ^{1}H NMR analysis indicated an isomeric mixture of adducts *viz.*, one isomer at δ 5.35 (br s, 1 H), 5.94 (br s, 1 H), 6.74 (d, 1 H) and 6.78 (d, 1 H) together with other isomers at δ 5.77 (dd, 1 H), 6.60 (m, 2 H), and 6.80 (m, 1 H) from vinylic and benzylic proton resonances only. Since the integration ratio of these protons with the aromatic protons (δ 7.3–7.8) was *ca.* unity, we inferred that adducts were formed in essentially quantitative yields. Work-up yielded pale yellow crystals [δ 5.34 (1 H), 5.94 (1 H), 6.74 (1 H), 6.78 (1 H), 7.20 (1 H), 7.54 (2 H) and 7.86 (1 H)] that were presumed to be the same as adduct **C** reported earlier.[14] When this crystalline adduct (8.0 μmol) was treated with wet acetonitrile, it was slowly converted into α-nitronaphthalene (GC, HPLC analysis) and nitroform (UV–VIS analysis, λ_{max} = 350 nm)[15] according to the stoichiometry in eqn. (7). The elimination occurred rapidly when aq. $NaHCO_3$ was added.[3]

When the charge-transfer nitration of naphthalene (0.11 mmol) and TNM (0.22 mmol) was carried out in 0.5 cm^3 of chloroform solution at $\lambda_{exc} > 480$ nm, it yielded a mixture of (α/β)-nitronaphthalene and adduct **C** (0.032 mmol) together with other isomers (0.066 mmol) according to ^{1}H NMR analysis. One-half of the photolysate was evaporated *in vacuo*, and triturated with *n*-pentane. HPLC analysis of the pentane extract for α/β-nitronaphthalenes is included in Table 2. Similarly, the treatment of naphthalene (0.091 mmol) and TNM (0.22 mmol) in 0.4 cm^3 of acetonitrile yielded the results listed in Table 2. In order to determine the total yield of α/β-nitronaphthalene and α/β adducts,[3] the charge-transfer nitration of naphthalene (0.15 mmol) and TNM (2.5 mmol) in 2 cm^3 of CH_3CN was repeated at $\lambda_{exc} > 425$ nm, and the photolysate evaporated *in vacuo*. The residue was dissolved in acetonitrile and treated directly with aq. $NaHCO_3$ to afford a mixture of α- (0.085 mmol) and β-nitronaphthalene (0.036 mmol). Repetition of the experiment in wet acetonitrile and in the presence of air yielded α- (0.059 mmol) and β-nitronaphthalene (0.011 mmol).

In the presence of 5–20 vol% trifluoroacetic acid, solutions of both $MeOPyNO_2^+$ and $C(NO_2)_4$ in acetonitrile remained colourless and were stable for at least a day. Furthermore, the charge-transfer complexes of naphthalene and $MeOPyNO_2^+$ (yellow-orange) or $C(NO_2)_4$ (red-orange) also persisted unchanged in the dark as judged by UV–VIS and ^{1}H NMR analysis. However, upon the deliberate irradiation at $\lambda_{exc} > 425$ nm, the CT colour bleached, and the spectral analysis of the photolysate yielded the products listed in Table 3. The prolonged monitoring of the ^{1}H NMR spectrum of the photolysate indicated that the adducts were unaffected by trifluoroacetic acid under these conditions.

Time-resolved Spectroscopy and the Spectral Decay of Naphthalene Cation Radicals.—Transient absorption spectra were obtained by the charge-transfer excitation at 355 nm of 0.1–0.2 mol dm^{-3} naphthalene and 0.01–0.04 mol dm^{-3} $MeOPy^+BF_4^-$ dissolved in acetonitrile and contained in a 1 cm quartz cuvette under an argon atmosphere. The corresponding TNM complex, prepared with 0.2–0.6 mol dm^{-3} naphthalene and 0.4–1.2 mol dm^{-3} tetranitromethane, was irradiated with λ_{exc} = 532 nm. The spectral decays were fitted to first-order, second-order or mixed first- and second-order decays using either the SLIDERITE PLUS (ps)[47] or ASYST 2.0[48] (ns/μs) software on an AT&T6300-plus microcomputer, as described previously.[27]

The decay kinetics of naphthalene cation radical in the presence of added pyridine, 2,6-lutidine and 2,6-di-*tert*-butyl-4-methylpyridine was followed at 580 nm subsequent to the 532 nm excitation of acetonitrile solutions containing 0.2 mol dm^{-3} naphthalene and 0.6 mol dm^{-3} TNM. The concentration of pyridine was varied incrementally from 3.0 to 20 mmol dm^{-3} and that of lutidine and di-*tert*-butylpicoline from 4.0 to 50 mmol dm^{-3}. For the decay kinetics in the presence of added NO_2, the scrupulously dried photochemical/electrochemical cell was filled with naphthalene and TNM in acetonitrile and the N_2O_4/NO_2 mixture was transferred *in vacuo via* a gas manifold. The concentration of NO_2 in solution was determined by the method of linear-sweep voltammetry, described earlier.[27] The potential of the microelectrode (r = 12.5 μm) was swept slowly positive at 0.05 V s^{-1}, and the anodic current due to NO_2 reached a steady-state value given by $i_{ss} = 4FD[NO_2]r$, where $D = 1.5 \times 10^{-5}$ cm^2 s^{-1} is the diffusion coefficient of NO_2,[44] r = 12.5 μm is the radius of the microelectrode, and F is the Faraday constant. Since the characteristic time $\tau = r^2/D$ was less than 0.1 s, the reversible dimerization was not a factor, and separate anodic waves of N_2O_4 and NO_2 were observed. As a check on this NO_2 determination, the absorption spectrum of the solution (in the absence of naphthalene) at λ = 420 and 440 nm[49] was examined, and the absorbance was found to be linear in the range: $0.1 < [NO_2] < 3.0$ mmol dm^{-3}. The acquisition of the kinetics data was limited to a few data points to avoid problems associated with the reaction of N_2O_4 with naphthalene.[50]

Quantum Efficiency for the CT Production of Naphthalene Cation Radical.—A benzene solution of benzophenone was

excited at 355 nm, and its transient triplet spectrum with λ_{max} = 530 nm and ε_T = 7220 dm^3 mol^{-1} cm^{-1} was monitored as the actinometer. A solution of 0.04 mol dm^{-3} $MeOPyNO_2^+$ and 0.1 mol dm^{-3} naphthalene in acetonitrile was irradiated at 355 nm, and the absorbance (A) of the transient $(NAPH)_2^{\bullet+}$ was determined on the timescale (0–20 μs) in which it persisted unchanged. The value of A was compared with the absorbance (A_0) of benzophenone triplet (generated from a sample with the same ground-state absorbance). According to the method of relative actinometry,[51] the quantum yield for $(NAPH)_2^{\bullet+}$ production is given by $\Phi = (A/A_0)$ (7220/ε), where the extinction coefficient of $(NAPH)_2^{\bullet+}$, ε = 3660 ± 200 dm^3 mol^{-1} cm^{-1}, was independently evaluated from naphthalene quenching of the chloranil triplet[16] with ε_{CA} = 9600 dm^3 mol^{-1} cm^{-1} at 450 nm.[52]

Appendix

The rate constant for the reaction of $(NAPH)^{\bullet+}$ with NO_2 was calculated from the observed decay of $(NAPH)_2^{\bullet+}$ as follows. The association rate constant (log k_a) and the formation constant (log K) evaluated by Rodgers[19] were plotted against the reciprocal temperature T^{-1}, and the extrapolation to T = 296 K yielded $k_a = 1.1 \times 10^{10}$ dm^3 mol^{-1} s^{-1} and K = 320 dm^3 mol^{-1} for eqn. (16). Letting [M] and [D] be the concentration of naphthalene cation radical monomer and dimer, respectively, [N] the concentration of naphthalene, and [A] the concentration of additive (either pyridine or NO_2), we obtain the steady-state expression (29) where k_2 is the

$$[M] = k_d[D]/(k_2[A] + k_a[N]) \quad (29)$$

calculated rate constant for eqn. (14). Since $k_a[N] \gg k_2[A]$, eqn. (29) reduces to $[M] = k_d[D]/k_a[N] = (K[N])^{-1}[D]$. The observed second-order rate is given by $k_{II}[D][A]$ which is equivalent to $k_2[M][A]$, and therefore $k_2 = k_{II}K[N]$. The values of k_2 in Table 7 were based on K = 320 dm^3 mol^{-1} and [N] = 0.2 mol dm^{-3}.

Acknowledgements

We thank the National Science Foundation, the Robert A. Welch Foundation and the Texas Advanced Research Project for financial assistance.

References

1 G. A. Olah, J. A. Olah and N. A. Overchuk, *J. Org. Chem.*, 1965, **30**, 3733; G. A. Olah, S. C. Narang, J. A. Olah, R. L. Pearson and C. A. Cupas, *J. Am. Chem. Soc.*, 1980, **102**, 3507.
2 E. K. Kim, K. Y. Lee and J. K. Kochi, *J. Am. Chem. Soc.*, 1992, **114**, 1756.
3 S. Sankararaman and J. K. Kochi, *J. Chem. Soc., Perkin Trans. 2*, 1991, 1.
4 K. Schofield, *Aromatic Nitration*, Cambridge University Press, New York, 1980.
5 G. A. Olah, R. Malhotra and S. C. Narang, *Nitration. Methods and Mechanisms*, VCH, New York, 1989.
6 C. L. Perrin, *J. Am. Chem. Soc.*, 1977, **99**, 5516.
7 (*a*) L. Eberson and F. Radner, *Acta Chem. Scand., Ser. B*, 1980, **34**, 739; (*b*) L. Eberson and F. Radner, *Acta Chem. Scand., Ser. B*, 1984, **38**, 861; (*c*) L. Eberson, L. Jönsson and F. Radner, *Acta Chem. Scand., Ser. B*, 1978, **32**, 749; (*d*) L. Eberson and F. Radner, *Acta Chem. Scand., Ser. B*, 1985, **39**, 343; (*e*) L. Eberson and F. Radner, *Acta Chem. Scand., Ser. B*, 1986, **40**, 71.
8 (*a*) A. Boughriet, C. Bremard and M. Wartel, *New J. Chem.*, 1987, **11**, 245; (*b*) A. Boughriet, C. Bremard and M. Wartel, *J. Electroanal. Chem.*, 1987, **225**, 125; (*c*) A. Boughriet and M. Wartel, *J. Chem. Soc., Chem. Commun.*, 1989, 809.
9 (*a*) J. F. Johnston, J. H. Ridd and J. P. B. Sandall, *J. Chem. Soc., Chem. Commun.*, 1989, 244; (*b*) A. H. Clemens, J. H. Ridd and J. P. B. Sandall, *J. Chem. Soc., Perkin Trans. 2*, 1985, 1227.
10 For a review: J. H. Ridd, *Chem. Soc. Rev.*, 1991, **20**, 149.
11 For example, see P. F. Barbara, L. E. Brus and P. M. Rentzepis, *Chem. Phys. Lett.*, 1980, **69**, 447; R. M. Hochstrasser, *Pure Appl. Chem.*, 1982, **52**, 2683; Y. Wang, M. K. Crawford and K. B. Eisenthal, *J. Phys. Chem.*, 1980, **84**, 2696.
12 J. D. Simon and K. S. Peters, *Acc. Chem. Res.*, 1984, **17**, 277; J. L. Goodman and K. S. Peters, *J. Am. Chem. Soc.*, 1985, **107**, 1441; 1986, **108**, 1700; E. O'Driscoll, J. D. Simon and K. S. Peters, *J. Am. Chem. Soc.*, 1990, **112**, 7091.
13 S. Sankararaman and J. K. Kochi, *J. Chem. Soc., Perkin Trans. 2*, 1991, 165.
14 L. Eberson, M. P. Hartshorn, F. Radner and W. T. Robinson, *J. Chem. Soc., Chem. Commun.*, 1992, 566.
15 (*a*) J. M. Masnovi, E. F. Hilinski, P. M. Rentzepis and J. K. Kochi, *J. Am. Chem. Soc.*, 1986, **108**, 1126; (*b*) S. Sankararaman, W. A. Haney and J. K. Kochi, *J. Am. Chem. Soc.*, 1987, **109**, 5235, 7824; (*c*) J. M. Masnovi, S. Sankararaman and J. K. Kochi, *J. Am. Chem. Soc.*, 1989, **111**, 2263.
16 R. Gschwind and E. Haselbach, *Helv. Chim. Acta*, 1979, **62**, 941.
17 T. Shida and W. H. Hamill, *J. Chem. Phys.*, 1966, **44**, 2375.
18 B. Badger and B. Brocklehurst, *Trans. Faraday Soc.*, 1969, **65**, 2588.
19 M. A. J. Rodgers, *J. Chem. Soc., Faraday Trans. 1*, 1972, **68**, 1278.
20 R. Bonneau, I. Carmichael and G. L. Hug, *Pure Appl. Chem.*, 1991, **63**, 289.
21 J. K. Hurley, N. Sinai and H. Linschitz, *Photochem. Photobiol.*, 1983, **38**, 9.
22 See the Experimental Section.
23 J. W. Moore and R. G. Pearson, *Kinetics and Mechanism*, 3rd edn., Wiley, New York, 1981, p. 60.
24 T. C. Hall, Jr. and F. E. Blacet, *J. Chem. Phys.*, 1952, **20**, 1745.
25 G. D. Gillispie and A. U. Kahn, *J. Chem. Phys.*, 1976, **65**, 1624.
26 See C. C. Addison, W. Karcher and H. Hecht, *Chemistry in Liquid Dinitrogen Tetroxide and Sulfur Dioxide*, Pergamon, New York, 1967, p. 37.
27 T. M. Bockman, Z. Karpinski, S. Sankararaman and J. K. Kochi, *J. Am. Chem. Soc.*, 1992, **114**, 1970.
28 Compare B. Reitstöen and V. D. Parker, *J. Am. Chem. Soc.*, 1991, **113**, 6954 and also refs. 15(*c*) and 31.
29 L. Melander, *Ark. Kemi*, 1950, **2**, 211; 1957, **11**, 77. See also L. Melander, *Isotope Effects on Reaction Rates*, Ronald Press, New York, 1960.
30 V. Enkelmann, *Adv. Chem. Ser.*, 1988, **217**, 177.
31 C. J. Schlesener and J. K. Kochi, *J. Org. Chem.*, 1984, **49**, 3142.
32 A. Fisher, W. J. Galloway and J. Vaughan, *J. Chem. Soc.*, 1964, 3591.
33 S. Ehrenson, R. T. C. Brownlee and R. W. Taft, *Prog. Phys. Org. Chem.*, 1973, **10**, 1.
34 Compare also J. M. Masnovi, S. Sankararaman and J. K. Kochi, in ref. 15(*c*).
35 See D. J. Cram, *Fundamentals of Carbanion Chemistry*, Academic, New York, 1965.
36 J. M. Masnovi and J. K. Kochi, *J. Am. Chem. Soc.*, 1985, **107**, 7880.
37 T. Yabe and J. K. Kochi, *J. Am. Chem. Soc.*, 1992, **114**, 4491.
38 Including both regio- and stereo-isomers.
39 E. K. Kim, T. M. Bockman and J. K. Kochi, *Bull. Soc. Chim. Fr.*, submitted for publication.
40 J. F. Johnston, J. H. Ridd and J. P. B. Sandall, *J. Chem. Soc., Perkin Trans. 2*, 1991, 623. See also J. H. Ridd in ref. 10.
41 L. Eberson and F. Radner, *Acc. Chem. Res.*, 1987, **20**, 53.
42 J. K. Kochi, *Acc. Chem. Res.*, 1992, **25**, 39.
43 E. K. Kim and J. K. Kochi, *J. Am. Chem. Soc.*, 1991, **113**, 4962.
44 K. Y. Lee, C. Amatore and J. K. Kochi, *J. Phys. Chem.*, 1991, **95**, 1285.
45 K. Y. Lee, T. M. Bockman and J. K. Kochi, *J. Chem. Soc., Perkin Trans. 2*, 1992, 1581.
46 For the concentration of the relevant EDA complex, see Kim *et al.* in ref. 2.
47 Advanced Graphics Software, Inc., 33 W. Maude Ave., Sunnyvale, CA 94086.
48 Macmillan Software Co., 866 Third Ave., New York, NY 10022.
49 M. Green in *Developments in Inorganic Nitrogen Chemistry*, vol. 1, ed. C. B. Colburn, Elsevier, New York, 1966, p. 1.
50 See L. Eberson and F. Radner, in ref. 7(*d*).
51 B. Amand and R. Bensasson, *Chem. Phys. Lett.*, 1975, **34**, 44.
52 J. J. Andre and G. Weill, *Mol. Phys.*, 1968, **15**, 97.

Paper 2/03564B
Received 6th *July* 1992
Accepted 12th *August* 1992